

# Enhancements of River Water Level Monitoring Method Using COSMO-SkyMed SAR Images

Francesco Forlingieri , *Graduate Student Member, IEEE*, Filippo Biondi , Nicomino Fiscante , Angelica Tarpanelli , Pia Addabbo , Carmine Clemente , *Senior Member, IEEE*, Gaetano Giunta , *Senior Member, IEEE*, and Danilo Orlando

**Abstract**—The problem of not having persistent river levels monitoring via satellite remote sensing is of considerable importance because the lack of this capability could affect the safety of inhabited areas near rivers. It has been shown that synthetic aperture radar (SAR) interferometry is a valid tool to measure the water surface of the river. Unfortunately, rivers can swell dynamically in less time than between two observations with the same geometric SAR parameters. Therefore, interferometric time series could not be used for effective emergency prevention and continuous monitoring because of geometric constraints. In this article, we propose an improvement of previous research by considering arbitrary geometric SAR acquisitions. The proposed method allows us to increase the possibility of image acquisition in order to drastically reduce the revisit time with respect to an interferometric acquisition strategy. Experimental results are consistent with the water level measurements from the *in situ* stations. Finally, the proposed procedure can potentially use data from any satellite system positioned in any orbit, not only sun-synchronous, in order to reduce time for more continuous monitoring of river levels.

**Index Terms**—COSMO-SkyMed Second Generation, river level monitoring, synthetic aperture radar (SAR).

## I. INTRODUCTION

RIVERS are a valuable source of water for all cities along their banks. Even today, in developing countries, rivers are used both as a source of drinking water and as a means of transport for people and goods, encouraging the development of residential centres close to watercourses, but also increasing the risk of flooding and overtopping. To mitigate hydraulic risk and better manage water resources, it is necessary to know the volume flowing through the watercourse, known as river discharge [1], by monitoring the water surface level of rivers [2]. However, *in situ* hydrometric monitoring networks are not evenly distributed

Manuscript received 16 August 2023; revised 16 April 2024; accepted 23 June 2024. Date of publication 2 July 2024; date of current version 24 July 2024. Corresponding author: Francesco Forlingieri.)

Francesco Forlingieri, Nicomino Fiscante, and Gaetano Giunta are with the Department of Industrial, Electronic and Mechanical Engineering, University of Roma Tre, 00146 Rome, Italy (e-mail: forlingieri.francesco@gmail.com).

Filippo Biondi and Carmine Clemente are with the University of Strathclyde, G11XW Glasgow, U.K.

Angelica Tarpanelli is with the National Research Council (CNR), Research Institute for Geo-Hydrological Protection (IRPI), 126-06128 Perugia, Italy.

Pia Addabbo is with the Viale Raffaele Delcogliano, University of Study Giustino Fortunato, 12-82100 Benevento, Italy.

Danilo Orlando is with the Department of Information Engineering, University of Pisa, 56122 Pisa, Italy.

Digital Object Identifier 10.1109/JSTARS.2024.3421998

around the world and many areas are often under-equipped [3]. For these reasons a space-based method for the measurements of water river level worldwide is a valid solution to provide river water level monitoring. The task of estimating the elevation of water flow through an original synthetic aperture radar (SAR) signal processing technique has been accomplished for the first time (at least to the best of authors' knowledge) in [4]. Due to the side-looking characteristics of SAR data acquisitions, bridges crossing rivers usually exhibit multiple bounce echoes in SAR images leading to multipath effects and range differences of the multiple returns that are proportional to the distances between the water surface and the bridge. Thus, the application of a new method for the design of a robust procedure to track over time the double-bounce reflections of bridges across rivers to measure the room existing between the river surface and the bridges is proposed and validated in [5] using *in situ* measurements. Measurements obtained from simulated as well as satellite time series of interferometric SAR data from COSMO-SkyMed (CSK), a constellation of small satellites positioned in a sun-synchronous orbit [6], [7], [8], [9], are compared with ground measurements recorded for three gauges and the experimental results confirms the effectiveness of water level estimation. The starting point of the algorithm proposed in [5] is a long temporal series of InSAR data but, instead of considering the deformations of the ground, it investigated the movements of the double-bounce scattering from man made structures localized on the water surface. Although the variations in water levels exhibit a faster dynamic with respect to the ground movements, Sub-Pixel Offset Tracking (SPOT), which is a relevant technique to measure large-scale ground displacements in both range and azimuth directions, is applied to trace their hydrometric levels. More recently, a method for estimating river water levels under bridges using multitemporal high resolution synthetic aperture radar intensity images at different incidence angles, was proposed in [10]. Range pixel distances are calculated using the cross correlation algorithm adopted in the SAR images coregistration, and then the water level oscillations are estimated. The main difference between [5] and [10] is that the algorithm proposed in [10] does not depend on the incidence angle between satellite and the bridge. Furthermore, they used the triple bounce for the river level estimation, but usually this phenomenon is composed by multiple reflections, because it depends on the bridge width, and it can be difficult to distinguish the exact range pixel difference between the bridge reflection and the triple bounce in the

presence of vegetation near rivers or angle of incidence near the axis of the bridge, as discussed in [5].

In this work, we want to overcome both the time limits of [5], caused by the interferometric configuration time gap, and those associated with the difficulty of distinguishing triple bounce for every incidence angle in [10]. Furthermore, we want to prove that, thanks to the independence of the geometry constraints, the algorithm proposed allows us to decrease revisit time in order to perform measurements closer in time with respect to [5]. COSMO-SkyMed Second Generation (CSG) satellites and their images are used for the aforementioned analysis because they have several advantages. As a matter of fact, CSG images have a better resolution with respect to CSK images, both in terms of ground range and azimuth resolution, allowing nonnegligible differences between single, double, and multiple bounces [11], [12]. The use of CSG allows for the exploitation of different geometric configurations between the target to be acquired and the satellite position [13], [14]. Specifically, there are four different modes of target acquisition: Right Ascending, Left Ascending, Right Descending, and Left Descending. The different possibilities of acquisition of a single CSG satellite allow for a reduction of the revisit-time by a factor 2 with respect to CSK, providing short reaction for alarms in case of emergencies. In fact, the interferometric time series of the CSK satellites lead to, in the best case, a revisit-time of 24 h, while using only a CSG satellite with different side looking acquisitions, it is possible to cut the revisit-time down almost by a factor of 2 in most of the cases. This time is further reduced by using two or more satellites per constellation. The proposed approach starts with the orthorectification and coregistration of the acquired images by using SARPROZ licensed software [15]. Such preliminary processing of CSG images allows us to exploit all the geometric configurations described above in order to reduce the revisit time. Furthermore, the co-registration of different orthorectified images on the same Digital Elevation Model (DEM), permits to use the SPOT technique, presented in [5], in order to calculate the ground range distance between single and double bounce. Thus, knowing the height of the bridge, we can estimate the river water level as described in Section II.

The rest of this article is organized as follows. Section II describes the methodology and related analytical aspects. Section III contains the experimental results. Finally, Section IV concludes this article.

*Notations:* The adopted notation uses boldface for vectors  $\mathbf{a}$ .  $\dot{\mathbf{a}}(x)$  and  $\ddot{\mathbf{a}}(x)$  denote the first and the second derivative of  $a(x)$  with respect to  $x$ , respectively.  $\mathbf{r}_{IJK}$  is the vector  $\mathbf{r}$  in the reference frame represented by the axes  $I, J, K$ .

## II. METHODOLOGY

The aim of this section is twofold. First, we provide the details required to calculate the time windows where the satellite is able to acquire images for a given area, with any geometry configuration, in order to estimate the revisit time. This is necessary because it allows us to estimate the incidence angles and to prove that a near real time river level monitoring via satellite

would be possible. Then, we describe the procedure to estimate river height. The entire processing chain starts with the images' acquisition with any geometry configuration and ends with the river height estimation from the images' set, taken at different incidence and look angles.

The orbit of CSG satellites is sun-synchronous, with repeating ground track and frozen perigee on the North Pole, with the same orbital parameters of CSK spacecrafts. This orbit can be mathematically modeled in order to perform a simulation of the Data Take Opportunity (DTO) which the constellation of satellites is able to acquire. A general Low Earth Orbit is modeled using a derivation of the Kepler equation, which is a solution of the two body problem perturbed by atmospheric drag, tesseral effects, due to the nonsphericity of the Earth, and other forces. These kinds of actions can be taken into account using the Cowell method [9]. This is the simplest and most straightforward of all the perturbation methods. The application of Cowell's procedure consists in writing the object motion's equations being studied, including all the perturbations, and successive integrations. For the two-body problem with perturbations, the equation is

$$\ddot{\mathbf{r}} + \frac{\mu}{r^3} \mathbf{r} = \mathbf{a}_p \quad (1)$$

where  $\mathbf{r}$ , whose intensity is given by  $r = (x^2 + y^2 + z^2)^{\frac{1}{2}}$ , is the instantaneous position vector of the satellite with respect to the Earth's centre;  $\mu$  is the universal gravity constant times the mass of the Earth;  $\mathbf{a}_p$  is in the form of an acceleration consisting of the sum of all physical perturbations that we named as  $p$ .

Rewriting (1) as

$$\dot{\mathbf{v}} = \mathbf{a}_p - \frac{\mu}{r^3} \mathbf{r}. \quad (2)$$

We can integrate  $\dot{\mathbf{v}}$  to obtain  $\dot{\mathbf{r}} = \mathbf{v}$ , where  $\mathbf{v}$  is the satellite velocity measured with respect to the Earth. Equation (2) can be written in terms of the velocity and acceleration scalar components as follows:

$$\begin{aligned} \dot{x} &= v_x, & \dot{v}_x &= a_{px} - \frac{\mu}{r^3} x, \\ \dot{y} &= v_y, & \dot{v}_y &= a_{py} - \frac{\mu}{r^3} y, \\ \dot{z} &= v_z, & \dot{v}_z &= a_{pz} - \frac{\mu}{r^3} z \end{aligned} \quad (3)$$

where  $x, y, z$  are the components of the satellite position vector in Earth Centered Inertial (ECI) reference frame. The change of the ECI reference frame into the Target-based reference frame can be achieved through a series of geometric transformations from ECI, whose axes are  $I, J, K$ , to the Topocentric-Horizon Coordinate System, whose axes are  $S, E, Z$  [8]. This coordinate transformations, can be performed using the angle of local sidereal time ( $\theta_{LST}$ ) and of the complementary of the geodetic latitude ( $\phi_{gd}$ ) [8]

$$\mathbf{r}_{IJK} = \begin{bmatrix} \cos(\theta_{LST}) & -\sin(\theta_{LST}) & 0 \\ \sin(\theta_{LST}) & \cos(\theta_{LST}) & 0 \\ 0 & 0 & 1 \end{bmatrix}$$

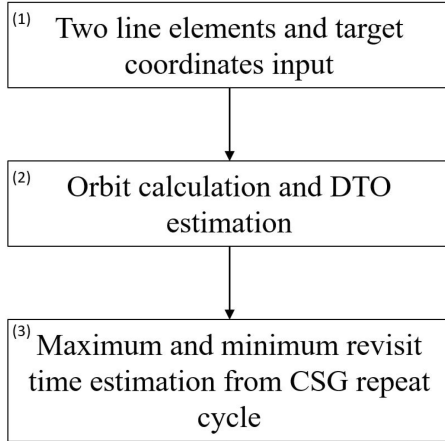


Fig. 1. Maximum and minimum revisit time simulation process.

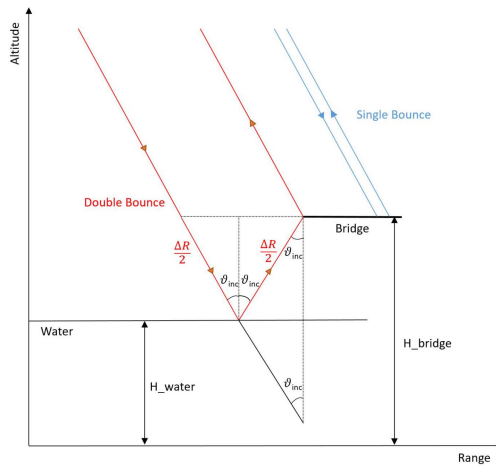


Fig. 2. Observation geometry for the river water flow elevation estimation: Ground range—height representation.

$$\begin{bmatrix} \cos(90 - \phi_{gd}) & 0 & \sin(90 - \phi_{gd}) \\ 0 & 1 & 0 \\ -\sin(90 - \phi_{gd}) & 0 & \cos(90 - \phi_{gd}) \end{bmatrix} \mathbf{r}_{SEZ}. \quad (4)$$

Fig. 1 describes the steps for the calculation of satellite's revisit time above the area of interest. Thus, using Two Line Elements input data in the planning algorithm, we calculate the DTO parameters for the target acquisition. As a matter of fact, (1)–(4) are used to calculate the time and the incidence angle needed by the satellite to acquire the image of the bridge over the river's water. Then, we plan the set of images in order to have the minimum revisit time between any geometry (Right Ascending, Left Ascending, Right Descending, Left Descending) acquisitions. The aim of this procedure is to provide evidence of the fact that, using any geometry, the revisit time dramatically decreases.

Now, we focus on the estimation of the water surface height. To this end, the geometry of the satellite position with respect to the bridge is depicted in Fig. 2. We assume that the electromagnetic waves coming from the SAR antenna are parallel

**Algorithm 1:** Computing Coefficients  $\alpha$  and  $\beta$  for  $\Gamma(n_{grp})_{\alpha,\beta}$  With a Single Image.

**Input:**  $\alpha_0, \beta_0, n_{grp}, \theta_{inc}$

**Output:**  $\alpha, \beta$

- 1: Set  $t = 0, \alpha^{(t)} = \alpha_0, \beta^{(t)} = \beta_0,$
- 2: Set  $t = t + 1$
- 3: Compute  $\Gamma_{\alpha,\beta}(n_{grp})^{(t-1)} = \alpha^{(t-1)}n_{grp} + \beta^{(t-1)}$
- 4: Compute

$$H_{water}^{(t-1)} = -\frac{\Gamma_{\alpha,\beta}(n_{grp})^{(t-1)} \cos \theta_{inc}}{2} + H_{bridge}$$

- 5: Compute

$$\eta = H_{water}^{(t-1)} - H_{ground-truth}$$

- 6: If  $|\eta| \geq 0.01$  and  $\eta < 0$  update  $\alpha^{(t)} = \alpha^{(t-1)} + 0.001$  and  $\beta^{(t)} = \beta^{(t-1)} - 0.001$  and go to step 2 else go to step 7
- 7: If  $|\eta| \geq 0.01$  and  $\eta > 0$  update  $\alpha^{(t)} = \alpha^{(t-1)} + 0.001$  and  $\beta^{(t)} = \beta^{(t-1)} + 0.001$  and go to step 2 else go to step 8
- 8: If  $0.001 < |\eta| < 0.01$  and  $\eta < 0$  update  $\beta^{(t)} = \beta^{(t-1)} - 0.0001$  and go to step 2 else go to step 9
- 9: If  $0.001 < |\eta| < 0.01$  and  $\eta > 0$  update  $\beta^{(t)} = \beta^{(t-1)} + 0.0001$  and go to step 2 else go to step 10
- 10: Return  $\alpha, \beta$

to the ones which come back to the satellite because of the large distance between the satellite position and the bridge. Furthermore, if the orientation of a bridge is not perpendicular to the orbit of the satellite, in high resolution SAR images different bright parallel stripes can be present, which represent: the direct backscatter from the bridge, the double bounce reflection between the bridge and water or vice versa, and the triple bounce reflection between the water, the lower part of the bridge, and the water again [10]. Single and double bounce are shown in Fig. 2. The time delay  $\Delta t$  of the double bounce with respect to the single bounce is  $\frac{2\Delta R}{c}$ , and this quantity is related to the difference between the height of the bridge ( $H_{bridge}$ ) and the height of the water ( $H_{water}$ ), and the angle of incidence of the electromagnetic wave coming from the satellite ( $\theta_{inc}$ ). The angle of incidence  $\theta_{inc}$  in (5) is computed using the previously described planning algorithm. Thus, in a CSG orbit cycle (16 d), we compute all the possible angles of incidence for CSG constellation with respect to the analyzed bridge. As a matter of fact, the angles used in the experimental results, which come from the real image set used for the analysis, will be a subset of all available incidence angles. From Fig. 2 we can write  $\Delta R$  as

$$\Delta R = 2(H_{bridge} - H_{water}) / \cos(\theta_{inc}). \quad (5)$$

In addition,  $\Delta R$  can be written as a linear metric function  $\Gamma_{\alpha,\beta}(n_{grp})$ , which depends on the number of ground range orthorectified image pixels between the single and the double bounce intensity reflection ( $n_{grp}$ ), and it has the coefficients  $\alpha, \beta$ , which are related to the estimation of the geometric distortion between orthorectified and single look complex (slant

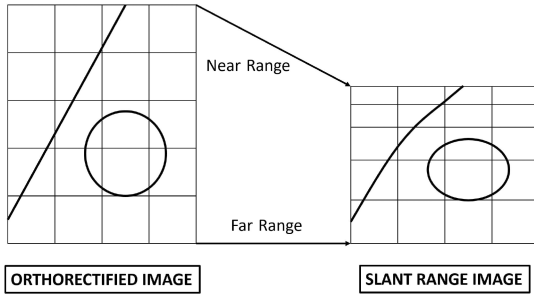


Fig. 3. Geometric distortions in SAR imagery.

range-azimuth plane) images. These coefficients are set during a training phase which is based on a conversion from ground range pixel to slant range pixel, through a comparison between initial value of river water level measurement and the ground range pixel distance between single and double bounce, in an image taken at the same time of the in situ measurements. In particular, we exploit (6) to estimate the coefficients of  $\Gamma_{\alpha,\beta}(n_{grp})$  from a subset of SAR images and ground truth. The logic flow is described by Algorithm 1 below. The threshold values can be chosen according to the uncertainty we want to have on the precision of the two different coefficients. The parameters  $\alpha$  and  $\beta$ , estimated via (6) which depends on the cosine of the angle of incidence, also vary as a function of the angle of incidence. If several test images are available for the estimation of  $\alpha$  and  $\beta$ , the algorithm is applied to each image that has a different angle of incidence. Then, once all coefficients have been calculated for each image, the final value of the coefficients for that particular bridge is obtained by averaging all the available estimates. The effect of  $\Gamma_{\alpha,\beta}(n_{grp})$ , related to the geometric distortion, caused by the transformation from ground range-azimuth plane to slant range-azimuth plane and viceversa, on the image's pixels is shown in Fig. 3. Orthorectification encompasses all the corrections needed to precisely align a SAR image to ground reference, accounting for actual topography [16], [19]. Thus, the expression that relates the water height with SAR image parameters can be written

$$H_{\text{water}} = -\frac{\Gamma_{\alpha,\beta}(n_{grp}) \cos(\theta_{\text{inc}})}{2} + H_{\text{bridge}}. \quad (6)$$

For the reader's ease, Fig. 4 describes the steps required for the computation of  $H_{\text{water}}$  starting from data collection acquired with the previous scheme. The images are orthorectified and then coregistered, in order to deal with different geometries of acquisition, for the multiple bounces information exploitation. Finally, through (6) the water river height is estimated from  $\Delta R$  using  $\Gamma_{\alpha,\beta}(n_{grp})$  conversion (ground range-azimuth to slant range-azimuth plane), the angles of incidence of the acquired images ( $\theta_{\text{inc}}$ ), and the bridge's height ( $H_{\text{bridge}}$ ).

### III. EXPERIMENTAL RESULTS

In this section, the performance of the entire processing procedure is assessed using two different datasets of 24 and 52 image acquisitions, respectively, with different geometric configurations to reduce the temporal gap between consecutive interferometric time series. The area of interest is located in

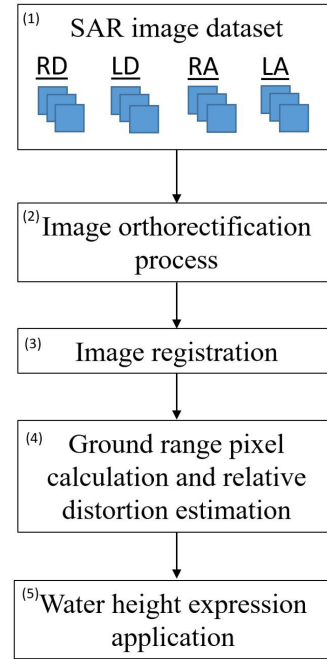


Fig. 4. Computational scheme of the river level monitoring algorithm.



Fig. 5. Optical image of the first analyzed bridge taken from Google Earth (48.5075°N, 107.2176°W).

Montana, United States of America, and contains two bridges on the Milk River whose coordinates are as follows:

- 1) 48.5075°N, 107.2176°W;<sup>1</sup>
- 2) 48.1235°N, 104.4748°W.

The optical images of the two areas of interest and of the analyzed sections (red lines) are provided in Fig. 5 and in Fig. 6, respectively. On the other hand, SAR images of both bridges are provided in Figs. 7 and 8. We estimate that the first bridge's height is 4.5 m, whereas the second bridge's height is 3.9 m with respect to NAVD-88 datum. The measure of the bridge height is only performed once by exploiting a geometrical relationship between the size of the bridge and the length of its shadow when it is adjacent to its pillar. In fact, by Pitagora's theorem we can estimate the bridge height as described in the Fig. 9. This

<sup>1</sup>The coordinates are given in the WGS-84 reference frame.



Fig. 6. Optical image of the second analyzed bridge taken from Google Earth (48.1235°N, 104.4748°W).

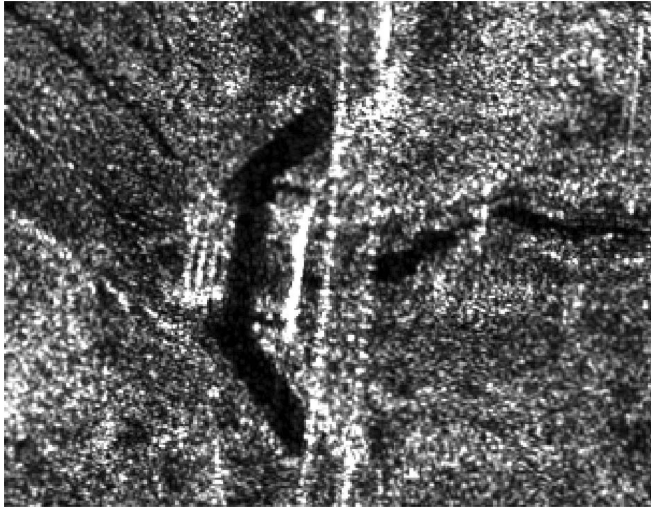


Fig. 7. SAR image of the first analyzed bridge (48.5075°N, 107.2176°W).

estimate can fail when the geometric misalignment between the bridge and its shadow is not negligible. However, any error on the bridge height estimate gives a translation error contribution in (6). R1C3—The error on the estimation of the bridge height can be mitigated by using the metric function  $\Gamma_{\alpha,\beta}(n_{\text{grp}})$  during the training phase for the selection of the coefficients  $\alpha$  and  $\beta$ . In fact, in the equation

$$\Gamma_{\alpha,\beta}(n_{\text{grp}}) = \alpha n_{\text{grp}} + \beta. \quad (7)$$

The coefficient  $\beta$  accounts for both translation displacement of the orthorectification process and the error, scaled by the factor  $\cos(\theta_{\text{inc}})/2$ , of the height bridge estimate. However, an exact height bridge measure is fundamental to return high accuracy estimates of the water height.

The observation time interval varies between September 2021 and December 2021 for the first bridge, and from September 2021 to February 2021 for the second bridge. The identification number of each image related to the incidence angle is shown in

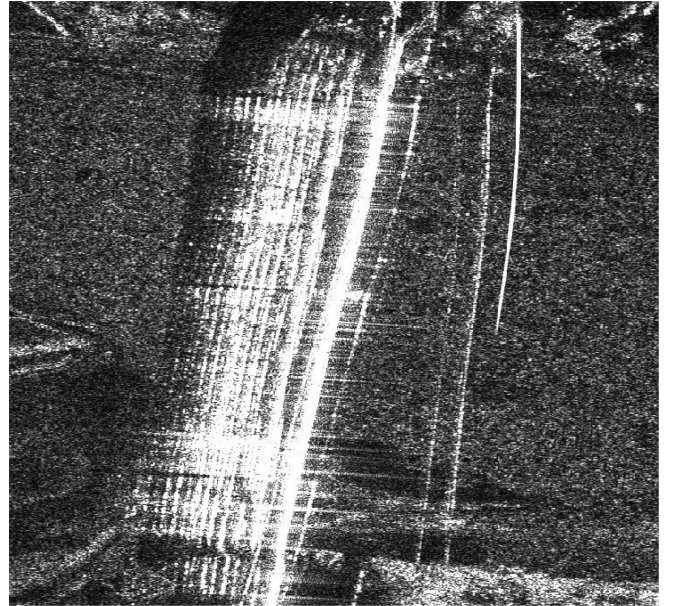


Fig. 8. SAR image of the second analyzed bridge (48.1235°N, 104.4748°W).

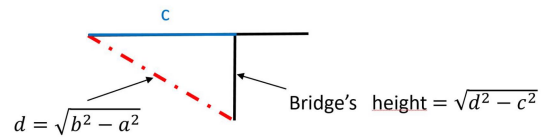
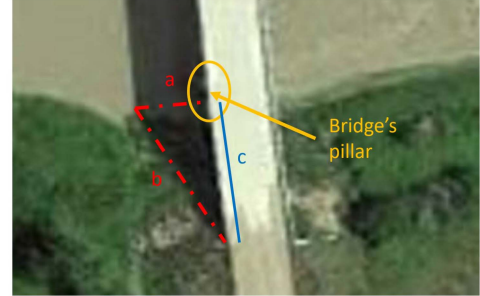


Fig. 9. Bridge's shadow exploitation for bridge's height estimation.

Table I for the first bridge analysis and in Table II for the second one.

The revisit times of COSMO constellation are computed according to (1)–(4) given in Section II. The maximum, minimum, and average revisit time of COSMO constellation for the two bridges, computed with: 1) three CSK operative satellites with only right looking side acquisition; 2) two CSG operative satellites with both left and right looking side acquisition; and 3) two CSG and three CSK operative satellites with the same constraints of the above items, are shown in Tables III and IV, respectively. The tables point out that using a combination of CSG and CSK satellites allows for short revisit times of the order of minutes.

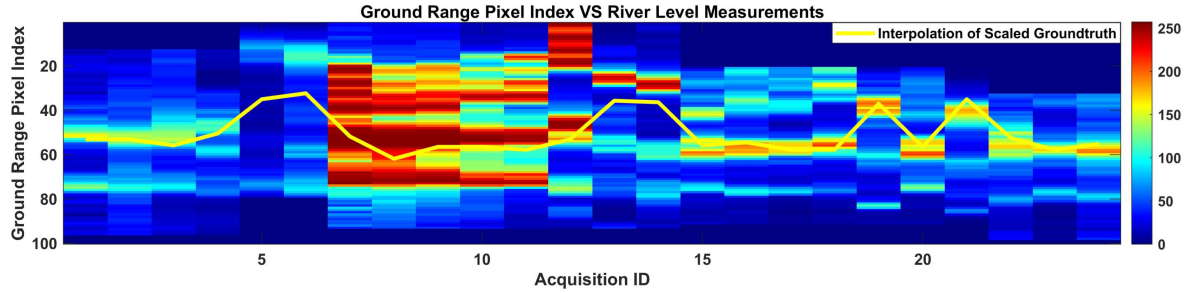


Fig. 10. Comparison between ground range pixel distance, which are mediated in azimuth direction, and river level measurements, scaled to pixel ground range unit of measurement, for each acquisition identification number of the first bridge analysis. The colorbar represents the intensity values of each ground range pixel.

TABLE I

IDENTIFICATION (ID) ACQUISITION NUMBERS AND THEIR RELATED INCIDENCE ANGLES, LOOK SIDE, AND ORBIT DIRECTION WITH RESPECT TO THE FIRST BRIDGE OF CSG ACQUISITIONS USED IN THE RIVER WATER LEVEL ESTIMATE

Acquisition ID	$\theta_{inc}$	Look Side	Orbit Direction
1	22.05°	Left	Ascending
2	45.425°	Left	Ascending
3	45.425°	Left	Ascending
4	55.35°	Left	Ascending
5	22.05°	Right	Descending
6	38.35°	Right	Descending
7	28.1°	Right	Descending
8	37.425°	Right	Descending
9	43.8°	Right	Descending
10	49.8°	Right	Descending
11	49.8°	Right	Descending
12	59.1°	Right	Descending
13	36.4°	Right	Descending
14	59.1°	Right	Descending
15	28.1°	Right	Ascending
16	29.15°	Right	Ascending
17	43.8°	Right	Ascending
18	43.8°	Right	Ascending
19	54.75°	Right	Ascending
20	54.75°	Right	Ascending
21	54.75°	Right	Ascending
22	31.35°	Left	Descending
23	55.35°	Left	Descending
24	57.1°	Left	Descending

In what follows, for simplicity and without lack of generality, we consider CSG satellites only. Focusing on the first bridge, Fig. 10 shows a comparison between the index of ground range pixel, which represents the distance from single to double bounce effect mediated in the azimuth direction, and the gauges measurements of the river level for each ID acquisition number. The CSG images identification number is shown on the x-axis, while on the y-axis the pixels' indices are arranged in the ground range direction from 1 to 100. Indeed, we consider a 100 range pixels window for each ID acquisition, whose intensity is averaged over a line of 10 pixels along the azimuth. Thus, each column (ID acquisition) of Fig. 10 represents 100 reflection intensity values in the range direction processed through a median filter, with the previous and the following five pixels in azimuth direction with respect to the section (red line) indicated in Fig. 5. The colors in Fig. 10 represent the different intensity values of the single bounces coming from the interaction with the edge's bridge and the double bounces caused by the bridge multipath effects. The detection and discrimination of single and

TABLE II

IDENTIFICATION (ID) ACQUISITION NUMBERS AND THEIR RELATED INCIDENCE ANGLES, LOOK SIDE, AND ORBIT DIRECTION WITH RESPECT TO THE SECOND BRIDGE OF CSG ACQUISITIONS USED IN THE RIVER WATER LEVEL ESTIMATE

Acquisition ID	$\theta_{inc}$	Look Side	Orbit Direction
1	23.28°	Left	Ascending
2	23.28°	Left	Ascending
3	23.28°	Left	Ascending
4	30.11°	Left	Ascending
5	36.87°	Left	Ascending
6	41.76°	Left	Ascending
7	41.76°	Left	Ascending
8	41.76°	Left	Ascending
9	41.76°	Left	Ascending
10	41.76°	Left	Ascending
11	46.17°	Left	Ascending
12	46.17°	Left	Ascending
13	46.17°	Left	Ascending
14	49.45°	Left	Ascending
15	20.01°	Left	Descending
16	20.01°	Left	Descending
17	20.01°	Left	Descending
18	20.01°	Left	Descending
19	27.33°	Left	Descending
20	39.81°	Left	Descending
21	39.81°	Left	Descending
22	44.65°	Left	Descending
23	44.65°	Left	Descending
24	48.1°	Left	Descending
25	51.45°	Left	Descending
26	23.28°	Right	Ascending
27	23.28°	Right	Ascending
28	23.28°	Right	Ascending
29	23.28°	Right	Ascending
30	23.28°	Right	Ascending
31	23.28°	Right	Ascending
32	23.28°	Right	Ascending
33	30.99°	Right	Ascending
34	30.99°	Right	Ascending
35	37.6°	Right	Ascending
36	37.6°	Right	Ascending
37	47.13°	Right	Ascending
38	47.13°	Right	Ascending
39	50.7°	Right	Ascending
40	50.7°	Right	Ascending
41	50.7°	Right	Ascending
42	18.84°	Right	Descending
43	27.33°	Right	Descending
44	33.64°	Right	Descending
45	33.64°	Right	Descending
46	44.65°	Right	Descending
47	48.57°	Right	Descending
48	48.57°	Right	Descending
49	51.83°	Right	Descending
50	51.83°	Right	Descending
51	51.83°	Right	Descending
52	51.83°	Right	Descending

TABLE III  
MAXIMUM, MINIMUM, AND AVERAGE REVISIT TIME OF SATELLITES' CONSTELLATION WITH RESPECT TO THE FIRST BRIDGE

No. Sat	Max. Rev.	Min. Rev.	Ave. Rev.
3 CSK	12 h 32 min 2 s	16 min 28 s	6h 36 min 32 s
2 CSG	12 h 32 min 3 s	47 min 27 s	5h 36 min 27 s
2 CSG + 3 CSK	12 h 19 min 42 s	10 min 27 s	3h 0 min 58 s

TABLE IV  
MAXIMUM, MINIMUM, AND AVERAGE REVISIT TIME OF SATELLITES' CONSTELLATION WITH RESPECT TO THE SECOND BRIDGE

No. Sat	Max. Rev.	Min. Rev.	Ave. Rev.
3 CSK	12 h 32 min 17 s	16 min 34 s	6 h 39 min 41 s
2 CSG	12 h 32 min 21 s	47 min 22 s	5 h 46 min 12 s
2 CSG + 3 CSK	12 h 31 min 47 s	10 min 32 s	3 h 09 min 35 s

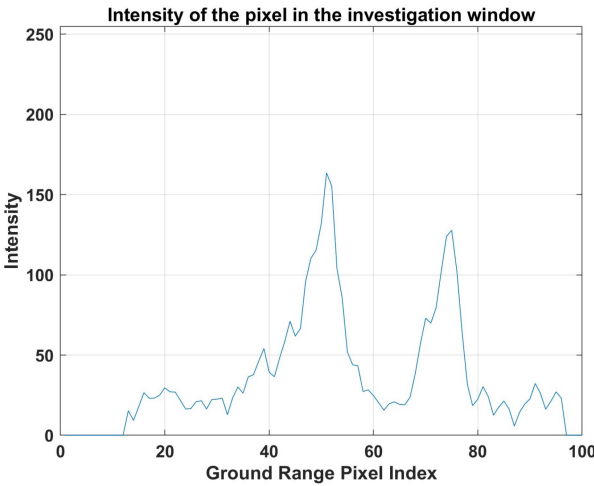


Fig. 11. Intensity profile of an image acquired under the Left-Ascending geometric configuration.

double bounces is grounded on the knowledge of the acquisition geometry since the satellite orbits as well as the bridge location are known. Specifically, in the case of Right-Descending (RD) and Left-Ascending (LA) configurations, the satellite looks at the bridge from the same side and the single, double, and triple bounces can be found in this order by moving from the right to the left part of the image. In the case of Right-Ascending (RA) and Left-Descending (LD) situations, the line of reasoning is the same as in the previous case except for the fact that the spatial sequence of bounces is reversed, namely they can be found moving from the left to the right part of the image. In Fig. 11, we show an intensity profile of an image acquired under the LA configuration and the first peak from the right represents the single bounce. It is detected by considering a subwindow of 30% of the investigation window width and selecting the maximum intensity within this subwindow. We perform the single bounce detection analysis on a reduced pixel window because we expect the single bounce to fall in the first 30% of pixels of the investigation window. This is because the investigation window is chosen to be in an area around the scattering phenomena of the bridge, and it can adapt to the different displacements due to image coregistration. Once the single bounce is located,

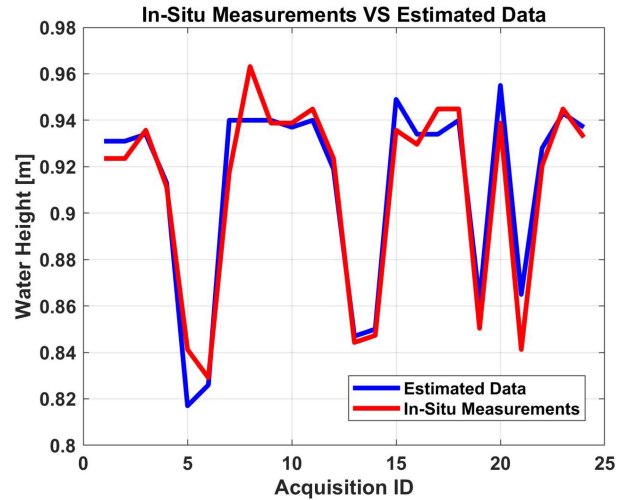


Fig. 12. Comparison between observed data and estimated data by satellite of the first bridge.

a detection threshold is set based upon the intensity value of the single bounce. More precisely, such a threshold is equal to the 90% of the single bounce intensity. Then, the threshold is applied to a subsequent window containing the remaining pixels and the pixels whose intensities are over the threshold are selected. The location of the double bounce is computed as the mean of such pixels. A similar analysis is conducted for RA and LD acquisitions but by placing the windows in a specular way. The yellow line represents the linear interpolation of the points returned by in situ river level measurements scaled to pixel ground range unit of measurements for each acquisition ID number. Notice that if we turn upside down this line and suitably scale it, we find the red line in Fig. 12, which is the ground truth. The yellow line in Fig. 10 follows the range pixels with the highest intensity. Notice that from ID 1 to ID 4, single and double bounces are very close to each other. This means that the water level is high because it is close to the edge's bridge. This fact is corroborated by Fig. 12 where we find a high value for the water level until ID 4. This situation is repeated for ID 7, 8, 9, 10, 11, 12, 15, 16, 17, 18, 20, 22, 23, 24. An opposite situation, i.e., high range pixel distance between single and double bounce, which means low water level, occurs for ID 5, 6, 13, 14, 19, 21.

It is important to notice that for some acquisitions the yellow line does not closely follow the maximum intensity path due to several reasons. For acquisitions with ID 5 and 6, this behavior might be due to residual errors associated with the transformation function  $\Gamma_{\alpha,\beta}(n_{grp})$  and/or the estimation accuracy for the bridge height. On the other hand, for acquisitions with IDs 7 to 11, the resulting intensity could also be due to the overlapping of different contributions (single, double, and triple bounces) contained in the window under investigation. The estimates of the water levels for the first bridge are shown in Fig. 12. The blue line represents the water-levels estimated by the proposed algorithms by using CSG satellite images and the red line represents the ground observation

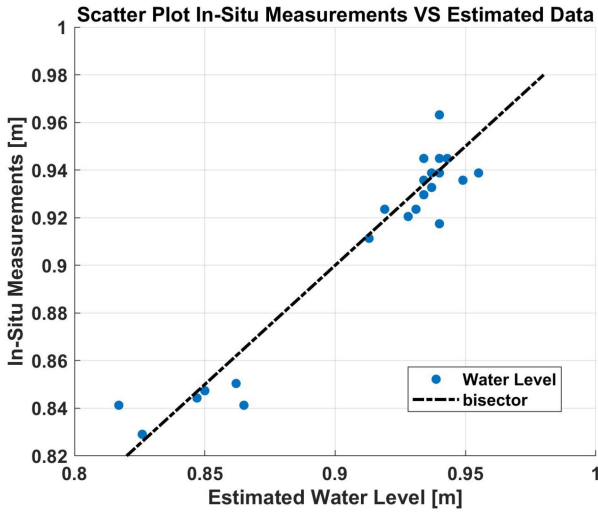


Fig. 13. Scatter plot of the water levels estimated by satellite and observed by in situ stations of the first bridge.

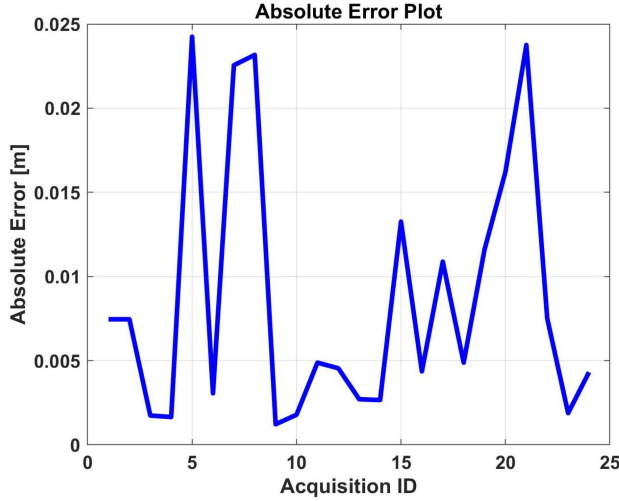


Fig. 14. Absolute Error Plot for each acquisition of the first bridge.

station [20]. The figure clearly points out that the SAR-based estimates closely follow the ground truth. In Fig. 13, the scatter plot is reported for the first area of interest, representing the comparison between the water levels estimated by the algorithm which exploits any geometry satellite images and those measured by the in situ station. In this case, almost all the blue points, that have both the in situ measurements and the estimated river level data as components, are very close to the bisector line, which indicates the location of points where the river level estimation, produced by the algorithm proposed in this article, is equal to the in situ measurements. The Absolute Error (AE) for each acquisition of the first bridge (blue line) is shown in Fig. 14. The maximum AE value is 0.025, thus the error is of the order of centimeters against a variation of decimeters.

Finally, we focus on the second bridge for which the comparisons between estimates from data and in situ measurements

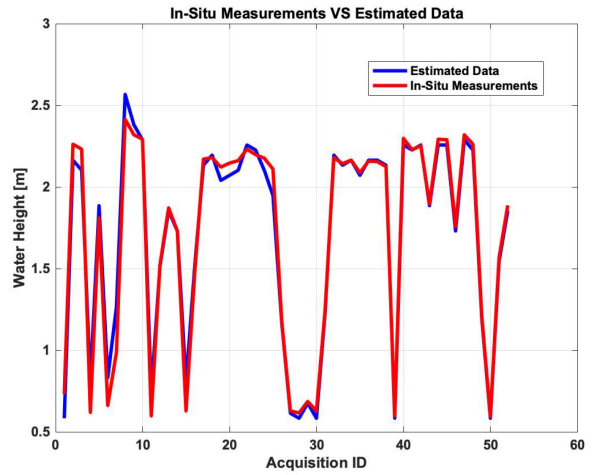


Fig. 15. Comparison between observed data and estimated data by satellite of the second bridge.

confirm the previously observed behavior. In fact, the overlap between such quantities is rather evident in Fig. 15. Fig. 16 shows a regular behavior as the yellow line, described in the previous plot, follows the intensity of the second bounce. The investigation window for the second bridge has a size of 150 pixels. This is necessary to take in account all the contributions of multiple bounces. In addition, at the bottom of the investigation window (last pixels) we have the contribution of the scattering given by the single bounce. In Fig. 17, the scatterplot is reported for the second area of interest, showing again that the estimates returned by the proposed approach are rightly concentrated around the bisector. The AE for each acquisition (blue line) of the second analysis is shown in Fig. 18, where the maximum AE value is 0.28. Thus, the error is of the order of decimeters against a variation of the order of meters.

Errors may be due to several causes. First, an inaccurate measurement of the height of the bridge can influence the estimate of the river level, even after the mitigation action associated with the translation factor  $\beta$ . Furthermore, although the analysis window is close to the centre of the bridge, in order to minimise the effects of other scattering traces (in addition to the bridge bounces), the considered rivers are very narrow, and, hence, the presence of vegetation on the river surface is likely and interferes with double and multiple bounces. As a consequence, the bounce detection algorithm might fail leading to an error in the estimation of the river level. In this case where the vegetation is on the surface of the river water, the double bounce location is estimated by averaging the pixels, related to the second subwindow described in Section II, whose intensity is above the detection threshold. Finally, poor coregistration between the images used to perform the water level estimation can generate an error on the pixel position in the image stack ( $n_{grp}$  is biased), which generates an error on the river water level estimate.

Summarizing, for both the considered bridges, the proposed method is capable of estimating the river height with an accuracy comparable with the in situ measurements.

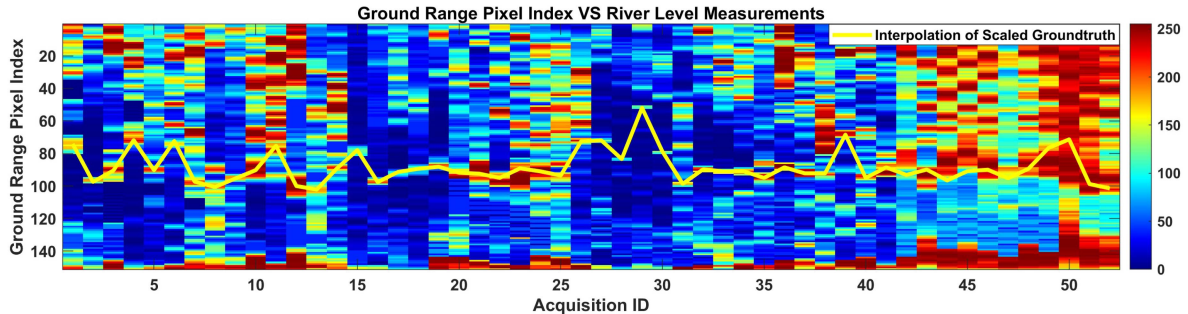


Fig. 16. Comparison between ground range pixel distance, which are mediated in azimuth direction, and river level measurements, scaled to pixel ground range unit of measurement, for each acquisition identification number of the second bridge analysis. The colorbar represents the intensity values of each ground range pixel.

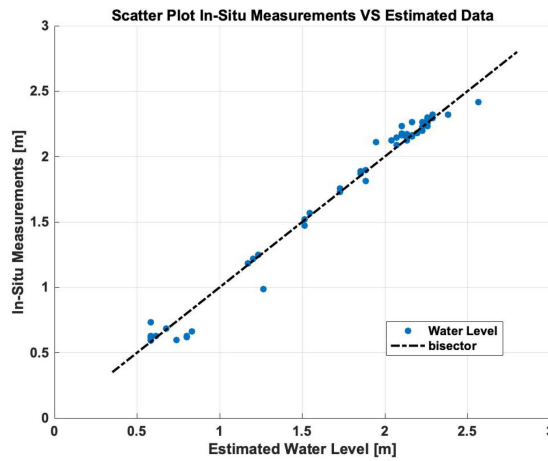


Fig. 17. Scatter plot of the water levels estimated by satellite and observed by in situ stations of the second bridge.

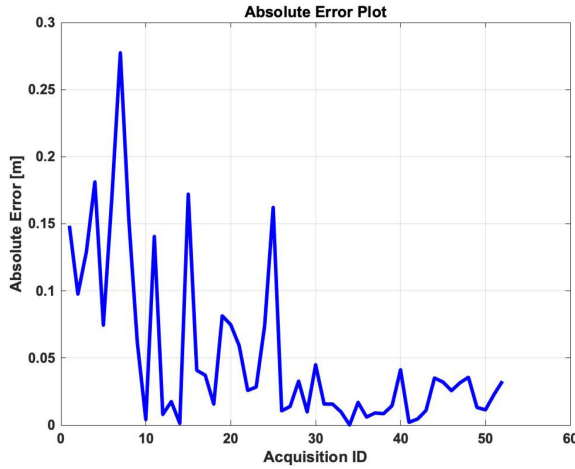


Fig. 18. Absolute Error Plot for each acquisition of the second bridge.

#### IV. CONCLUSION

In this article, an enhancement of the procedure for estimating the water flow elevation of rivers in terms of reduction of revisit time with respect to [4] has been proposed. In fact, nowadays, many areas are still unmonitored and the time gap for interferometric passages is too large for an effective emergency prevention. The proposed approach represents an effective means to solve the above problem by exploiting a high number

of satellite noninterferometric acquisitions over a certain area. To face the problems related to different acquisition geometries, the images are first orthorectified and then the distance between the double-bounce reflections and direct backscattered echoes from the principal structures of the bridge is computed. Such a distance is suitably used to obtain the water height estimates. Remarkably, this method allows us to use all possible satellite acquisition opportunity for a given area of interest with the consequent reduction of the revisit time. In the numerical example of the first and second bridge, a time interval of 16 d is considered (i.e., the CSK and CSG repeat cycle), using both CSK and CSG satellites, the revisit time for the first bridge, is reduced from 8 d (interferometric time gap if we have two satellites on the same orbit positioned with a phase of 180° between them) to 12 h 19 min and 42 s for the worst case scenario, and from 24 h (interferometric time gap if we have two satellites on the same orbit positioned with a phase of 66.7° between them) to 10 min 27 s. These results have been obtained by processing both CSK and CSG orbital data, while the experiments related to the algorithm for river level measurements estimation have been performed by processing a CSG dataset, courtesy of the Italian Space Agency. It is important to highlight that the proposed procedure provides reliable results when it is fed by SAR images sharing a range-azimuth resolution at least comparable with the bridge size. This aspect prevents the use, for instance, of images acquired by Sentinel-1. Another important caution related to the proposed procedure is that in some situations the presence of clutter due to vegetation over the bridge can mask the single and/or double bounces. As explained in Section III, in such a case, a procedure to mitigate clutter effects is required with a consequent impairment of the performance.

The proposed approach could be analyzed in a structured manner on a large dataset including more challenging situations to better substantiate the limits of applicability.

#### ACKNOWLEDGMENT

The authors would like to thank the Italian National Research Council—Research Institute for Geo-Hydrological Protection for the in situ measurements data, which have been used as ground-truths for the estimate of  $\Gamma_{\alpha,\beta}(n_{grp})$  and the validation of the proposed river water level method. We would like to thank also the Italian Space Agency for the CSG image dataset used for the whole analysis.

## REFERENCES

- [1] B. M. Fekete, R. D. Robarts, M. Kumagai, H. P. Nachtegel, E. Odada, and A. V. Zhulidov, "Time for in situ renaissance," *Science*, vol. 349, no. 6249, pp. 685–686, 2015.
- [2] F. Biondi et al., "Water level measurement using COSMO-SkyMed synthetic aperture radar," in *Proc. IEEE 7th Int. Workshop Metrol. AeroSpace*, 2020, pp. 148–153.
- [3] D. M. Hannah et al., "Large-scale river flow archives: Importance, current status and future needs," *Hydrol Process*, vol. 25, no. 7, pp. 1191–1200, 2011.
- [4] D. E. Alsdorf, C. L. Smith, and J. M. Melack, "Amazon floodplain water level changes measured with interferometric SIR-C radar," *IEEE Trans. Geosci. Remote Sens.*, vol. 39, no. 2, pp. 423–431, Feb. 2001.
- [5] F. Biondi et al., "Pixel tracking to estimate rivers water flow elevation using Cosmo-SkyMed synthetic aperture radar data," *Remote Sens.*, vol. 11, no. 21, 2019, Art. no. 2574.
- [6] M. Virelli, A. Coletta, and M. L. Battagliere, "ASI COSMO-SkyMed: Mission overview and data exploitation," *IEEE Geosci. Remote Sens. Mag.*, vol. 2, no. 2, pp. 64–66, Jun. 2014.
- [7] M. Martorella, D. Pastina, F. Berizzi, and P. Lombardo, "Spaceborne radar imaging of maritime moving targets with the Cosmo-SkyMed SAR system," *IEEE J. Sel. Topics Appl. Earth Observ. Remote Sens.*, vol. 7, no. 7, pp. 2797–2810, Jul. 2014.
- [8] D. A. Vallado, *Fundamentals of Astrodynamics and Applications*, vol. 12. Hawthorne, CA: Springer, 2001.
- [9] R. R. Bate et al., *Fundamentals of Astrodynamics*. New York, NY, USA: Courier Dover Publications, 2020.
- [10] X. Chen et al., "Monitoring river water level using multiple bounces of bridges in SAR images," *Adv. Space Res.*, vol. 68, no. 10, pp. 4016–4023, 2021.
- [11] F. Caltagirone, "Architecture and evolution of COSMO-SkyMed," *Space Mag.*, vol. 2, no. 5, pp. 24–33, 2014.
- [12] [Online]. Available: <https://www.asi.it/wp-content/uploads/2021/02/CSG-Mission-and-Products-Description-issue-A-1.pdf>
- [13] D. Calabrese et al., "CSG system performance and mission," in *Proc. EUSAR 11th Eur. Conf. Synthetic Aperture Radar*, 2016, pp. 1–4.
- [14] S. Mari et al., "The Mission simulator of COSMO-SkyMed di seconda generazione: A valuable tool supporting the Developing, verification and operational phases of the programme". [Online]. Available: [https://indico.esa.int/event/180/contributions/1341/attachments/1269/1494/1230\\_Mari\\_-\\_Paper.pdf](https://indico.esa.int/event/180/contributions/1341/attachments/1269/1494/1230_Mari_-_Paper.pdf)
- [15] D. Perissin, Z. Wang, and T. Wang, "The SARPROZ InSAR tool for urban subsidence/manmade structure stability monitoring in China," in *Proc. ISRSE*, 2011, Art. no. 1015.
- [16] L. Pierce et al., "Practical SAR orthorectification," in *Proc. IEEE Int. Geosci. Remote Sens. Symp.*, 1996, vol. 4, pp. 2329–2331.
- [17] G. M. Huang et al., "Algorithms and experiment on SAR image orthorectification based on polynomial rectification and height displacement correction," in *Proc. Int. Arch. Photogrammetry, Remote Sens. Spatial Inf. Sci.*, 2004, vol. 34.
- [18] R. Hu, B. S. M. R. Rao, M. Alaei-Kerahroodi, and B. Ottersten, "Orthorectified polar format algorithm for generalized spotlight SAR imaging with DEM," *IEEE Trans. Geosci. Remote Sens.*, vol. 59, no. 5, pp. 3999–4007, May 2021.
- [19] M. Esmaeilzade, J. Amini, and S. Zakeri, "Georeferencing on synthetic aperture RADAR imagery." international archives of the photogrammetry," *Remote Sens. Spatial Inf. Sci.*, vol. 1, pp. 179–184, 2015.
- [20] [Online]. Available: <https://snoflo.org/report/flow/montana/milk-river-at-juneberg-bridge-nr-saco-mt/>



**Francesco Forlingieri** (Graduate Student Member, IEEE) was born in Rome, Italy, on April 20, 1994. He received the M.Sc. degree (cum laude) in aerospace engineering from the University of Naples "Federico II," Naples, Italy, in 2019, and the second-level master's degree (cum laude) in satellite systems and services from the University of Rome "La Sapienza," Rome, Italy, in 2021. He is currently working toward the Ph.D. degree in applied electronics with the University of Roma TRE, Rome.

His research interests include satellite remote sensing for Earth observation, GIS, and statistical signal processing for synthetic aperture radar data applications.



**Filippo Biondi** was born in L'Aquila, Italy, in 1974. He received the B.S. degree in information engineering and the M.S. degree in telecommunication engineering from Salento University, Lecce, Italy, in 2009 and 2011, respectively, and the Ph.D. degree in telecommunication engineering from the University of L'Aquila, L'Aquila, Italy, in 2015.

From 2010 to 2011, he was Guest Scientist with the Nation Research Council (ISSIA-CNR) of Bari Italy and the Italian Space Agency, Geodesy Space Center of Matera Italy. He is currently working on synthetic aperture radar (SAR), interferometry, multichromatic analysis, and tomography, also using a Convex Optimization approach. His research interests include the development of signal processing and statistical signal processing techniques on radar equipment.



**Nicomino Fiscante** was born in Benevento, Italy, in 1982. He received the M.Sc. degree (cum laude) in telecommunication engineering from the University of Sannio, Benevento, Italy, in 2007, and the Ph.D. degree in applied electronics from the University of Roma TRE, Italy, in 2023.

From January to June 2007, he was a Trainee with the Antenna Group, Netherlands Organization for Applied Scientific Research (TNO Defense, Security, and Safety), The Hague, Netherlands. From 2008 to 2012, he was with Mediterranean Agency for Remote Sensing and Environmental Control (MARSec), Benevento, Italy. From 2012 to 2014, he was with Advanced Research Technology Spa in Passignano sul Trasimeno, Italy. Since 2014, he has been a Project Manager with Geoslab (now GeneGIS GI), where he has gained extensive work experience both nationally and internationally through collaborations with major companies, research centers, universities, and institutions. His research interests include remote sensing, GIS, data processing, TLC and EM systems, mobile mapping systems, and renewable resources.



**Angelica Tarpanelli** received the M.S. and the Ph.D. degrees in hydraulic engineering from the University of Perugia, Perugia, Italy, in 2006 and 2014, respectively.

From 2012 to 2022, she was a Researcher, and since 2023, Senior Researcher with National Research Council, Research Institute for Geo-Hydrological Protection of (CNR-IRPI), Perugia. She actively participated (as responsible and coordinator) to several research projects in the frame of Italian and European programs and funded by International space agencies, in collaboration with Italian and International institutions. Her research activities mainly regard the development and implementation of algorithms for hydrological and hydraulic applications through the leveraging of satellite sensors data. She has a long background on the estimation of river discharge as a key variable of the water cycle through the combination of multimission data. Her research interests include the hydraulic risk assessment through in situ and remote sensing data, the design flood estimation for water management and flood hazard assessment, and the exploration of the potential of soil moisture for the quantification of the irrigation.

Dr. Tarpanelli is a Member of the Italian Hydrological Society (IHS), Hydraulic Group (GII), the European Geophysical Union (EGU), and the American Geophysical Union (AGU).



**Pia Addabbo** received the B.Sc. and M.Sc. degrees in telecommunication engineering and the Ph.D. degree in information engineering from the Università degli Studi del Sannio, Benevento, Italy, in 2005, 2008, and 2012, respectively.

She is currently an Associate Professor with the Giustino Fortunato University, Benevento. She is the coauthor of scientific publications in international journals and conferences. Her research interests include statistical signal processing applied to radar target recognition, Global Navigation Satellite System reflectometry, and hyperspectral unmixing.

Dr. Addabbo is currently an Associate Editor for IEEE ACCESS and *Scientific Reports*.



**Carmine Clemente** (Senior Member, IEEE) received the B.Sc. (laurea cum laude) and M.Sc. (laurea specialistica cum laude) degrees in telecommunications engineering from Università degli Studi del Sannio, Benevento, Italy, in 2006 and 2009, respectively, and the Ph.D. degree in signal processing from the University of Strathclyde, Glasgow, U.K., in 2012.

He is currently a Professor of radar systems and signal processing with the Department of Electronic and Electrical Engineering, University of Strathclyde, where he is the Director of the Sensor Signal Processing and Security Laboratories. His research interests include advanced radar/SAR signal processing algorithms, distributed and MIMO radars, passive radar systems, and micro-Doppler analysis, extraction, and classification.

Dr. Clemente is a recognized expert in micro-Doppler signatures from radar and has delivered several tutorials on the topic at international conferences. He is the Co-Chair of the Advanced Signal Processing for Radar and EW focus Group of the Electromagnetic Systems Interest Group - the UK Radar society.



**Danilo Orlando** was born in Gagliano del Capo, Italy, in 1978. He received the Dr. Eng. degree (with honors) in computer engineering and the Ph.D. degree (with maximum score) in information engineering from the University of Salento (formerly University of Lecce), Lecce, Italy, in 2004 and 2008, respectively.

From 2007 to 2010, he was with the University of Cassino, Cassino, Italy, engaged in a research project on algorithms for track-before-detect of multiple targets in uncertain scenarios. From September to November 2009, he was a Visiting Scientist with

the NATO Undersea Research Centre, La Spezia, Italy. From 2011 to 2015, he was with Elettronica S.p.A. engaged as System Analyst in the field of electronic warfare. From 2015 to 2024, he joined Università degli Studi "Niccolò Cusano," Rome, Italy, as an Associate Professor. From 2024, he is an Associate Professor with the Department of Information Engineering, Università degli Studi di Pisa, Pisa, Italy. In 2007, he has held visiting positions with the Department of Avionics and Systems, ENSICA (now Institut Supérieur de l'Aéronautique et de l'Espace (ISAE)), Toulouse, France, and from 2017 to 2019, with the Chinese Academy of Science, Beijing, China. He has authored or coauthored more than 190 scientific publications in international journals, conferences, and books. His main research interests include statistical signal processing with more emphasis on adaptive detection and tracking of multiple targets in multisensor scenarios.

Dr. Orlando was Senior Area Editor for *IEEE TRANSACTIONS ON SIGNAL PROCESSING* and is currently an Associate Editor for *IEEE Open Journal of Signal Processing*, *IEEE TRANSACTIONS ON AEROSPACE AND ELECTRONIC SYSTEMS*, *EURASIP Journal on Advances in Signal Processing*, and *Remote Sensing (MDPI)*.



**Gaetano Giunta** (Senior Member, IEEE) received the degree in electronic engineering from the University of Pisa, Pisa, Italy, in 1985, and the Ph.D. degree in information and communication engineering from the University of Rome La Sapienza, Rome, Italy, in 1990.

Since 1989, he has been a Research Fellow with the Signal Processing Laboratory (LTS), EPFL, Lausanne, Switzerland. In 1992, he was an Assistant Professor with the INFO-COM Department, University of Rome La Sapienza. From 2001 to 2005, he was with the University Roma Tre, Rome, as an Associate Professor. Since 2005, he has been a Full Professor of telecommunications with the University Roma Tre, where he currently teaches the courses "Digital Signal Processing," "Signal Processing for Biomedical Engineering," and "Mobile Communications." His research interests include signal processing for mobile communications, image communications, and security.

Dr. Giunta has been a Member of the IEEE Societies of Communications, Signal Processing, and Vehicular Technology. He has served as a Reviewer for several IEEE Transactions, IET (formerly IEE) proceedings, and EURASIP journals, and a TPC Member for several international conferences and symposia in the abovementioned fields.

Open Access funding provided by 'Università degli Studi Roma Tre' within the CRUI CARE Agreement